ARTICLE

Efficient Near-Infrared Quantum Cutting in Tm^{3+}/Yb^{3+} Codoped $LiYF_4$ Single Crystals for Solar Photovoltaic

Li Fu[a], Hai-ping Xia[a*], Yan-ming Dong[a], Shan-shan Li[a], Xue-mei Gu[a], Jian-li Zhang[a], Dong-jie Wang[a], Hao-chuan Jiang[b], Bao-jiu Chen[c]

a. Key laboratory of Photoelectronic Materials, Ningbo University, Ningbo 315211, China
b. Ningbo Institute of Materials Technology and Engineering, the Chinese Academy of Sciences, Ningbo 315211, China
c. Department of Physics, Dalian Maritime University, Dalian 116026, China

(Dated: Received on July 16, 2014; Accepted on January 11, 2015)

Downconversion (DC) with emission of two near-infrared photons about 1000 nm for each blue photon absorbed was obtained in thulium (Tm^{3+}) and ytterbium (Yb^{3+}) codoped yttrium lithium fluoride ($LiYF_4$) single crystals grown by an improved Bridgman method. The luminescent properties of the crystals were measured through photoluminescence excitation, emission spectra and decay curves. Luminescence between 960 and 1050 nm from Yb^{3+}: $^2F_{5/2}\rightarrow{}^2F_{7/2}$ transition, which was originated from the DC from Tm^{3+} ions to Yb^{3+} ions, was observed under the excitation of blue photon at 465 nm. Moreover, the energy transfer processes were studied based on the Inokuti-Hirayama model, and the results indicated that the energy transfer from Tm^{3+} to Yb^{3+} was an electric dipole-dipole interaction. The maximum quantum cutting efficiency approached up to 167.5% in $LiYF_4$ single crystal codoped with 0.49mol% Tm^{3+} and 5.99mol% Yb^{3+}. Application of this crystal has prospects for increasing the energy efficiency of crystalline Si solar cells by photon doubling of the high energy part of the solar spectrum.

Key words: Quantum cutting, Energy transfer, $LiYF_4$ single crystals, Tm^{3+}/Yb^{3+}

I. INTRODUCTION

In recent decades, quantum cutting downconversion, which is based on the principle that it is theoretically possible to divide one high energy ultraviolet (UV) photon into two near-infrared photons [1], has attracted great attention as potential application in photovoltaic solar cells. Downconversion has been realized in many rare earths ion couples such as Tb^{3+}/Yb^{3+}, Pr^{3+}/Yb^{3+}, and Nd^{3+}/Yb^{3+} to convert visible photons into near-infrared photons [1−6], which can modify the solar spectrum to increase the conversion efficiency of sunlight to electricity. The theoretically optical quantum efficiency can be close to 200%.

Downconversion of Tm^{3+}/Yb^{3+} ions has also been experimentally realized for a cooperative energy transfer (ET) from Tm^{3+} ($^1G_4\rightarrow{}^3H_5$) to two Yb^{3+} ($^2F_{7/2}\rightarrow{}^2F_{5/2}$) ions in $GdAl_3(BO_3)_4$ by Zhang *et al.* in 2007 [2]. Due to abundant energy levels of Tm^{3+} in the range of UV-visible and good energy match between Tm^{3+} ($^1G_4\rightarrow{}^3H_5$) and Yb^{3+} ($^2F_{7/2}\rightarrow{}^2F_{5/2}$), it is easy to realize the downconversion for Tm^{3+}/Yb^{3+} codoped solid materials. After that, downconversion has been experimentally realized from many Tm^{3+}/Yb^{3+} couples codoped in powders, micro-crystals or glasses [8−11].

The downconversion of Tm^{3+}/Yb^{3+} couples is also dependent on the host material. However, because of adversity of light scattering for the powders and the low luminous efficiency of rare earth ions and low chemical stability, glasses are deficient to be applied effectively in solar cells and other optical devices [5, 12]. As host matrix of downconversion materials, the single crystal has the advantage of excellent comprehensive properties. The $LiYF_4$ single crystals are excellently favorable as the host materials for practical applications in optical devices due to their low phonon energy, relatively high optical damage threshold, and good thermal, mechanical, and excellent chemical stability [5].

In this work, we chose $LiYF_4$ single crystal as matrix for Tm^{3+} and Yb^{3+} ions because of the very near ionic radii between Tm^{3+} (0.87 Å) and Y^{3+} (0.893 Å), and Yb^{3+} (0.858 Å) and Y^{3+}. It is expected that a moderately homogenous distribution for Tm^{3+} and Yb^{3+} in $LiYF_4$ single crystal can be obtained. The inhomogenous concentration of rare earths ions resulting from their distribution phenomenon in single crystal strongly influences the quality of crystal and practical applications.

*Author to whom correspondence should be addressed. E-mail: hpxcm@nbu.edu.cn

Generally, the rare earth ions are dispersed in the network of glass. Unlike in glass matrix, the rare earth ions Tm^{3+} and Yb^{3+} substitute Y^{3+} ions in a non-centersymmetrical site, and they have undergone a strong interaction from the crystal field of $LiYF_4$, which exerts an effective influence on the optical spectra and quantum cutting for rare earths. However, the quantum cutting optical properties of Tm^{3+}/Yb^{3+} codoped $LiYF_4$ single crystals are not known well yet.

We have reported the absorption and fluorescence spectra of Pr^{3+}/Yb^{3+} and Tb^{3+}/Yb^{3+} codoped $LiYF_4$ single crystal grown by Bridgman method, in which the maximum downconversions were 168.4% and 166.7%, respectively [2, 5]. In this work, we examines the doping concentration effects on quantum efficiency from the VIS and near-infrared emissions and decay lifetimes data. An efficient near-infrared emission quantum cutting downconversion and quantum efficiency from the Tm^{3+}/Yb^{3+} codoped $LiYF_4$ single crystals were determined.

II. EXPERIMENTS

The feed materials for Tm^{3+}/Yb^{3+}: $LiYF_4$ crystals were synthesized with molar compositions of 0.515LiF-0.005TmF_3-(0.48−x)YF_3-$x$$YbF_3$ (x=0.00, 0.02, 0.04, 0.06, 0.08, and 0.10). The raw materials (YF_3, LiF, TmF_3, and YbF_3 powders) with 99.999% of purity were weighed according to formula $LiY_{0.995-x}Tm_{0.005}Yb_xF_4$. In this work, Tm^{3+}/Yb^{3+}:$LiYF_4$ crystals were grown with a modified Bridgman method and the particular process of this method has been reported in our previous work [5]. In order to obtain high quality single crystals, feed materials for crystals growth were prepared with a slight excess of LiF.

Tm^{3+}/Yb^{3+} codoped $LiYF_4$ single crystals with high quality grown by Bridgman method were about 10 mm in diameter and 105 mm in length as shown in the left of Fig.1. These crystals were transparent and flavescent. It is obvious that the color changed slightly along the growth direction. The top of the crystals are dark yellow and lighttight due to the constituent of other impurities and redundant LiF. In order to measure the optical features conveniently, the crystals were cut into small pieces and polished on both sides to about 2.3 mm thickness, as shown in the right of Fig.1.

The structures of the crystals were investigated by X-ray diffraction (XRD) using a XD-98X diffractometer (XD-3, Beijing). The absorption spectra of Tm^{3+}/Yb^{3+} ions were measured in 300−1300 nm interval using a Cary 5000 UV/VIS/NIR spectrophotometer (Agilent Co., America). The excitation and emission spectra and decay curves were obtained with a FLSP 920 type spectrometer (Edinburgh Co., England). Moreover, the concentrations of Tm^{3+}/Yb^{3+} ions in the $LiYF_4$ single crystals were measured by inductively coupled plasma atomic emission spectroscopy (ICP-AES, PerkinElmer lnc., Optima 3000). The concentration of different samples are shown in Table I. The samples with different Tm^{3+} and Yb^{3+} concentrations were designated TY0, TY1, TY2, TY3, TY4, and TY5, respectively. All of the measurements were performed at room temperature.

FIG. 1 Tm^{3+}/Yb^{3+} codoped $LiYF_4$ single crystal (left) and polished crystal (right).

TABLE I Concentrations of Tm^{3+} ions and Yb^{3+} ions in the single crystals.

Samples	Concentration/mol%					
	TY0	TY1	TY2	TY3	TY4	TY5
Tm^{3+}	0.49	0.48	0.49	0.49	0.50	0.49
Yb^{3+}	0.00	1.96	3.98	5.99	7.97	9.98

III. RESULTS AND DISCUSSION

The XRD pattern and the established cell parameters for $LiYF_4$ sample codoped with 0.49mol% Tm^{3+} and 5.99mol% Yb^{3+} are shown in Fig.2(a). For comparison, the peak positions and the cell parameters of $LiYF_4$ in JCPD 77-0816 are displayed in Fig.2(b), one can confirm that the current doping level does not cause any obvious peak shift or second phase and the crystal is pure orthorhombic phase. In Fig.2(a), the crystal cell parameters are computed from the XRD spectrum. The result displays that the variable of cell volume is only 0.004 nm and cell volume negligible change is 1.38%. It authenticates that $LiYF_4$ single crystals do not occur any obvious transform in structure when those ions are doped. The similar XRD patterns we obtained from 0.5mol% Tm^{3+} and different Yb^{3+} doping concentrations suggest that most samples have been crystallized into the pure orthorhombic phase. Moreover, it can also be ensured that the Y^{3+} ions sites of $LiYF_4$ single crystals were substituted by Tm^{3+} and Yb^{3+} ions.

The absorption coefficient spectra of sample TY0 and TY1 in region of 300−1300 nm are presented in Fig.3. The absorption spectrum of $LiYF_4$ crystal has no visible absorption bands in this region [2]. The most obvious absorption band of TY1 from 910 nm to 1030 nm, which is different from TY0, attributed to the transition $^2F_{7/2}\rightarrow{}^2F_{5/2}$ of Yb^{3+} in $LiYF_4$ crystal. Meanwhile, a strong absorption peak at 465 nm is attributed to the transition Tm^{3+}: $^3H_6\rightarrow{}^1G_4$. One can be convinced that these single crystals can be pumped efficiently by a 465 nm light. It is coincident that the wavelength at

DOI:10.1063/1674-0068/28/cjcp1407115

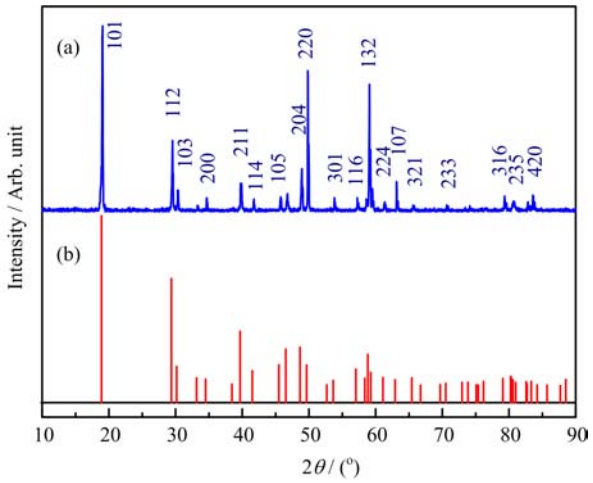

FIG. 2 (a) Powder XRD pattern of the $LiYF_4$:Tm^{3+}/Yb^{3+} crystal, a=0.5153 nm, b=0.5153 nm, c=1.0674 nm. (b) The standard line pattern of orthorhombic phase $LiYF_4$ (JCPD 77-0816), a=0.5171 nm, b=0.5171 nm, c=1.0748 nm.

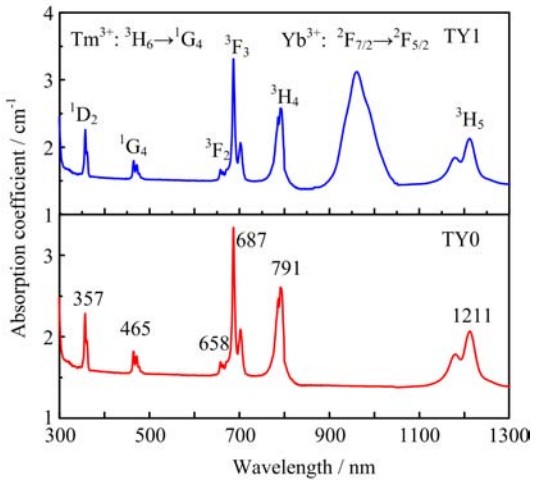

FIG. 3 Absorption coefficient spectra of the Tm^{3+} doped crystal (TY0) and Tm^{3+}/Yb^{3+} codoped crystal (TY1).

465 nm is half of the mated wavelength with transition of Yb^{3+}: $^2F_{7/2}\rightarrow{}^2F_{5/2}$. Moreover, others absorption bands centered at 357, 658, 687, 791, and 1211 nm correspond to the transitions of Tm^{3+} from the ground state ($^3H_6$) to $^1D_2$, $^3F_2$, $^3F_3$, $^3H_4$, and $^3H_5$, respectively.

Figure 4 presents the excitation and emission spectra of all samples. In the photoluminescence excitation spectra of 0.48mol% Tm^{3+} and 1.96mol% Yb^{3+} codoped $LiYF_4$ sample, strong excitation bands at 465 nm are detected by monitoring both the Tm^{3+}: $^1G_4\rightarrow{}^3F_4$ transition at 646 nm and Yb^{3+}: $^2F_{5/2}\rightarrow{}^2F_{7/2}$ transition at 980 nm. The excitation appearances indicate the occurrence of energy transfer from Tm^{3+} to Yb^{3+} because that the incident light at 465 nm can not be absorbed by the spectral mismatched Yb^{3+} ions.

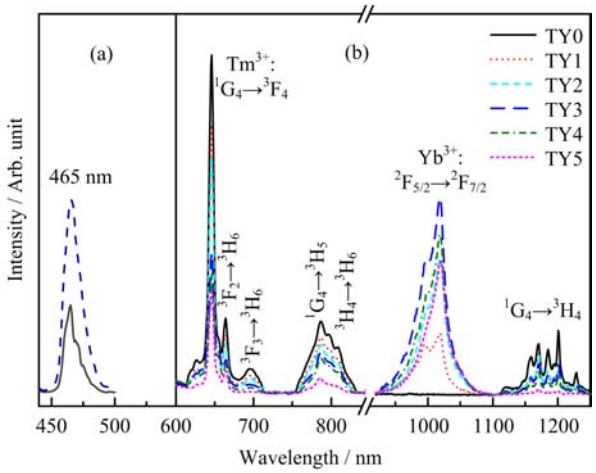

FIG. 4 (a) Photoluminescence excitation spectra of Tm^{3+} 646 nm emission (dash line) and Yb^{3+} 980 nm emission (solid line) in sample TY1. (b) Emission spectra upon excitation of 465 nm in all samples.

Furthermore, the photoluminescence spectra for samples with the concentrations of Yb^{3+} ions varying from 0mol% to 9.98mol%, are collected under blue light excitation at 465 nm laser diode corresponding to the Tm^{3+}: $^3H_6\rightarrow{}^1G_4$ transition. The most intense emission peak is at 646 nm, corresponding to $^1G_4\rightarrow{}^3F_4$ transition of Tm^{3+} ions [13]. Other assigned bands about 696 nm ($^3F_3\rightarrow{}^3H_6$), 787 nm ($^1G_4\rightarrow{}^3H_5$), 808 nm ($^3H_4\rightarrow{}^3H_6$), and 1171 nm ($^1G_4\rightarrow{}^3H_4$) are also checked in every sample [13]. Those emission bands are multiple and sharp due to the energy splitting in crystal [2]. And an intense emission band in the region from 960 nm to 1050 nm can be observed when Yb^{3+} ions are codoped into Tm^{3+}-$LiYF_4$ crystal. This emission band around 1000 nm is attributed to the transitions from the stark level $^2F_{5/2}$ multiplet of Yb^{3+} to the stark level $^2F_{7/2}$ multiplet appearances. When the concentrations of Yb^{3+} are improved from 0mol% to 9.98mol%, the Tm^{3+} concentration is held approximately to about 0.49mol%, the emission of Tm^{3+} decreases monotonically. Moreover, the NIR emissions of Yb^{3+} first intensify significantly and then attenuate in pace with increased concentration of Yb^{3+}. And the decrease in the near-infrared emission has been clearly observed as a result of concentration quenching [3]. The emission intensity reaches a maximum when the Yb^{3+} concentration is 5.99mol%. In addition, only Tm^{3+} ions can absorb the excitation light at 465 nm to jump to the excited state from the ground state in the Tm^{3+}/Yb^{3+} codoped $LiYF_4$ crystal. Meanwhile, the observation for both the emissions from transitions of Tm^{3+} and Yb^{3+} ions upon excitation at 465 nm, further confirms the occurrence of ET from Tm^{3+} to Yb^{3+}.

In order to illustrate the quantum cutting downconversion process in Tm^{3+}/Yb^{3+} codoped $LiYF_4$ definitely, the schematic energy level diagram with involved

DOI:10.1063/1674-0068/28/cjcp1407115

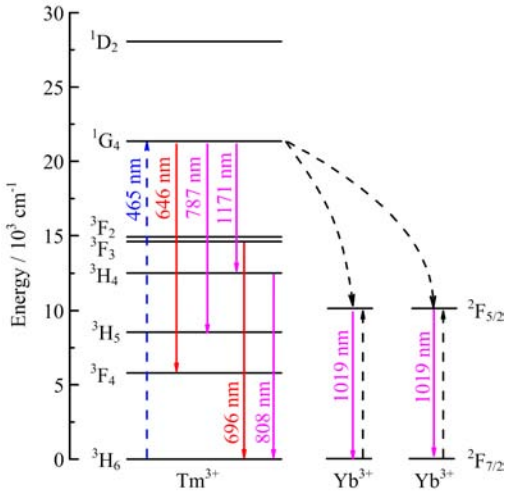

FIG. 5 Partial energy level diagram of Tm^{3+} and Yb^{3+} ions and the cooperative transfer mechanism of $Tm^{3+}(^1G_4)\rightarrow Yb^{3+}(^2F_{7/2})$ in Tm^{3+} and Yb^{3+} ions codoped $LiYF_4$ crystals are indicated by dash curve lines.

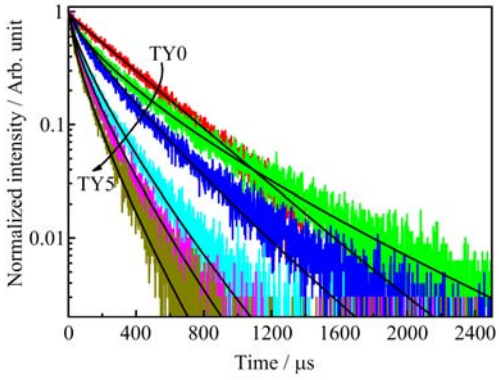

FIG. 6 Decay curves of the Tm^{3+}/Yb^{3+} codoped $LiYF_4$ crystal samples are monitored at 646 nm under the 465 nm excitation. The black solid lines are the stretched exponential fits for the decays.

TABLE II Luminescence decay parameters, mean decay lifetime τ_m, energy transfer efficiency η_{ETE}, and quantum efficiency η_{QE} for Tm^{3+} and Yb^{3+} codoped in $LiYF_4$ single crystal samples (TY0−TY5).

Sample	τ_m/μs	τ/μs	β	η_{ETE}/%	η_{QE}/%
TY0	344.0	343.8	1.00		
TY1	262.9	212.0	0.91	23.6	123.6
TY2	199.2	185.4	0.83	42.1	142.1
TY3	111.7	99.2	0.77	67.5	167.5
TY4	91.2	79.2	0.75	73.5	173.5
TY5	72.1	58.4	0.73	79.1	179.1

cooperative energy transfer process between Tm^{3+} ions and Yb^{3+} ions is depicted in Fig.5. One Tm^{3+} ion can transfer its energy to two Yb^{3+} ions or radiate to the lower energy states with emissions under the excitation of 465 nm light since the $^1G_4$ level of Tm^{3+} is located approximately twice the energy for $^2F_{5/2}$ of Yb^{3+} as shown in Fig.5. We can express the cooperative downconversion mechanism with a process: $Tm^{3+}(^1G_4)+2Yb^{3+}(^2F_{7/2})\rightarrow Tm^{3+}(^3H_6)+2Yb^{3+}(^2F_{5/2})$. One Tm^{3+} ion radiates with the emissions at the range from 600 nm to 900 nm and around 1171 nm as shown in Fig.4 or transfers its energy to two Yb^{3+} ions, under irradiation at 465 nm. Moreover, it is not possible that resonant energy transfer is from a Tm^{3+}:$^1G_4$ state to one Yb^{3+}, since the Yb^{3+} ion has only one excited state around 1000 nm and no transition from Tm^{3+}:$^1G_4$ is suitable to match the gap of it. So little phonon energy about 425 cm^{-1} of the $LiYF_4$ single crystal compared with the energy difference between $^1G_4$ state of Tm^{3+} and $^2F_{5/2}$ state of Yb^{3+} about 10974 cm^{-1} that the phonon assisted energy transfer process is almost excluded. Then the cooperative quantum cutting downconversion process from one Tm^{3+} ion to two Yb^{3+} ions to explain this energy transfer process is reasonable. In this quantum cutting process, the quantum efficiency up to 200% is possible theoretically, because the energy of a visible photon absorbed about 21505.4 cm^{-1} is more than twice that of a near-infrared photon emission about 9813.5 cm^{-1} from Yb^{3+} ions.

The decay curves of the Tm^{3+}: $^1G_4\rightarrow{}^3F_4$ luminescence at 646 nm in Tm^{3+}/Yb^{3+} codoped $LiYF_4$ single crystals are plotted in Fig.6. And the solid lines are the stretched exponential fitting for the decays. As Table II shows, the decay curve of 0.49mol% Tm^{3+} singly doped $LiYF_4$ sample is close to single exponential. However, the decay lifetimes decrease rapidly from 344 μs to 72.1 μs with an increase in the Yb^{3+} concentrations from 0mol% to 9.98mol%. Meanwhile, the energy transfer from Tm^{3+} to Yb^{3+} appearances and the decay curves become non-exponential. For the non-exponential emission decay of these samples, the mean decay lifetime (τ_m) is calculated by [4]:

$$\tau_m = \frac{1}{I_0}\int I(t)\mathrm{d}t \qquad (1)$$

where $I(t)$ is the recorded luminescence intensity as a function of time t, and I_0 represents the maximum of $I(t)$ which occurs at the initial time t_0. Moreover, the decay curves are well described by the stretched exponential function (often called a Kohlrausch function) shown below [5, 14]:

$$I(t) = I_0 \exp\left[-\left(\frac{t}{\tau_{ch}}\right)^{\beta}\right], \quad 0<\beta<1 \qquad (2)$$

where $I(t)$ is equal to I_0 at t=0, the parameters τ_{ch} and β depend on the material and can be a function of external variables like temperature [14]. In this work, τ_{ch} gives a characteristic lifetime for the decay of the excited states of Tm ions. The β parameter is the degree to which the measured decay differs from a purely

DOI:10.1063/1674-0068/28/cjcp1407115

exponential decay. The obtained parameters τ_{ch} and β are also listed in Table II. It is clear that both parameters τ_{ch} and β are reduced with increasing of Yb^{3+} concentration when the concentration of Tm^{3+} is held constant at ~0.49mol%. One can confirm the energy transfer from Tm^{3+} to Yb^{3+} ions existence in these samples.

The energy transfer efficiency (η_{ETE}) is defined as the ratio of donors that are depopulated by energy transfer to the acceptors over the total number of donors being excited. Here, Tm^{3+} acts as the donor and Yb^{3+} as the acceptor. The η_{ETE} is obtained as a function of the Yb^{3+} concentration as follows:

$$\eta_{ETE} = \eta_{x\%Yb} = 1 - \frac{\int I_{x\%Yb}dt}{\int I_{0\%Yb}dt} \quad (3)$$

where I stands for the decay intensity of 646 nm at time t and x%Yb denotes the Yb^{3+} content. Additionally, the total quantum efficiency (η_{QT}) can be defined as the ratio of the emitted photons to the photons that are absorbed, assuming that all excited Yb^{3+} ions decay radiatively. This assumption leads to an upper limit of the quantum efficiency, and the actual quantum efficiency may be lower due to concentration quenching [4]. The relation between η_{ETE} and η_{QE} is linear and defined as [9],

$$\eta_{QE} = \eta_{Tm}(1 - \eta_{ETE}) + 2\eta_{ETE} \quad (4)$$

where η_{QE} is the quantum efficiency for the Tm^{3+} ions. Giving no consideration to the nonradiative energy loss by defects and impurities, η_{Tm} is set to 1 [1, 3]. The values of η_{ETE} and η_{QE} are also summarized in Table II.

It can be confirmed from Table II, when concentration of Tm^{3+} is held about 0.49mol%, both η_{ETE} and η_{QE} are monotonously increasing from 23.6% to 79.1% and 123.6% to 179.1%, respectively, with the increase of Yb^{3+} concentration from 1.96mol% to 9.98mol%. However, taking into account the concentration quenching of Yb^{3+}, the actual QE would be lower [3]. Since quantum efficiency and the 0.49mol%Tm^{3+}/5.99mol%Yb^{3+} codoped $LiYF_4$ crystal reach near-infrared emission maximum intensity, the maximum quantum efficiency should be 167.5% in all samples.

In order to research the energy transfer mechanism, we use the Inokuti-Hirayama model to commentate the energy transfer mechanism of the non-exponential fluorescent decay. This model can express the decay curves as [2, 15]:

$$I(t) = \exp\left[\frac{-t}{\tau_0} - \frac{4\pi}{3}\Gamma\left(1 - \frac{3}{s}\right) {R_0}^3 N \left(\frac{t}{t_0}\right)^{3/s}\right] \quad (5)$$

where τ_0 is the intrinsic radiation lifetime, R_0 is the critical transfer distance, N denotes the concentration, and

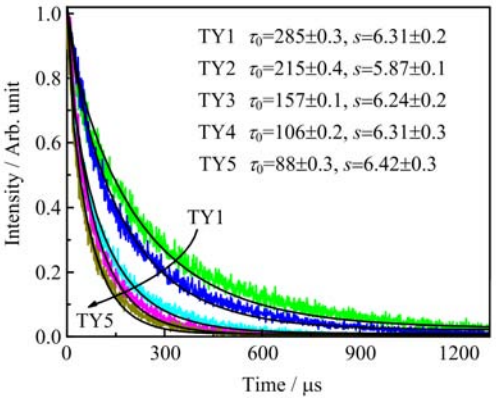

FIG. 7 Decay curves of the Tm^{3+}/Yb^{3+} ions codoped $LiYF_4$ crystal samples are monitored at 646 nm under the 465 nm excitation. The black solid lines are the Inokuti-Hirayama model fitting results for the decays.

$\Gamma(1 - 3/s)$ is a Gamma function. Here, the parameter s=6, 8, and 10, respectively, denote the electric dipole-dipole, dipole-quadrupole, and quadrupole-quadrupole interactions between luminescent centers [2, 5, 15]. The $\Gamma(1 - 3/s)$ will be 1.77, 1.43, and 1.30 when s=6, 8, and 10, respectively. The fitting curves are shown in Fig.7. The values of τ_0 decrease rapidly with the increase of Yb^{3+} concentration, implying a fast energy transfer from Tm^{3+} to Yb^{3+} since the interaction of Yb^{3+} and Tm^{3+} changes from long to short distance. However, the τ_0 from the data fitting with $s \approx 6$ consistently means the energy transfer of electric dipole-dipole interaction from Tm^{3+} to Yb^{3+} in $LiYF_4$ single crystal.

IV. CONCLUSION

Our experiments demonstrate that there is a distinct near-infrared emission about 1000 nm from Tm^{3+}/Yb^{3+} codoped $LiYF_4$ single crystal prepared by Bridgman techniques excited by a 465 nm light. A high energy transfer efficiency from Tm^{3+} to Yb^{3+} ions in $LiYF_4$ crystal is confirmed from recorded absorption, luminescence spectra (excitation and emission), and luminescence decay curves. The Yb^{3+} ions emit two near-infrared photons about 1000 nm through energy transfer from Tm^{3+} to Yb^{3+}, with maximum quantum efficiency as high as 167.5% for $LiYF_4$: 0.49mol%Tm^{3+}/5.99mol%Yb^{3+} sample, under excitation of blue photon at 465 nm. These Tm^{3+}/Yb^{3+} codoped $LiYF_4$ single crystals are promising materials for applications in solar cells since the advantages of better optical properties, efficient near-infrared quantum cutting, and stable chemical properties.

V. ACKNOWLEDGMENTS

This work was supported by the National Natural Science Foundation of China (No.51472125 and

DOI:10.1063/1674-0068/28/cjcp1407115

No.51272109) and K. C. Wong Magna Fund in Ningbo University.

[1] L. Fu, H. Xia, Y. Dong, S. Li, H. Jiang, and B. Chen, IEEE Photon. J. **6**, 2600209 (2014).
[2] Q. Y. Zhang, G. F. Yang, and Z. H. Jiang, Appl. Phys. Lett. **91**, 051903 (2007).
[3] Q. Y. Zhang, C. H. Yang, Z. H. Jiang, and X. H. Jiang, Appl. Phys. Lett. **90**, 061914 (2007).
[4] G. Lakshminarayana and J. Qiu, J. Alloy Compd. **481**, 582 (2009).
[5] J. Hu, H. Xia, H. Hu, Y. Zhang, H. Jiang, and B. Chen, J. Appl. Phys. **112**, 073518 (2012).
[6] J. Sun, Y. Sun, Z. Xia, and H. Du, Appl. Phys. B **111**, 367 (2013).
[7] D. L. Dexter, Phys Rev. **108**, 630 (1957).
[8] Q. Y. Zhang and X. F. Liang, J. Soc. Inform. Display. **16**, 755 (2008).
[9] L. Xie, Y. Wang, and H. Zhang, Appl. Phys. Lett. **94**, 061905 (2009).
[10] G. Lakshminarayana, H. C. Yang, S. Ye, Y. Liu, and J. R. Qiu, J. Phys. D **4**, 175111 (2008).
[11] S. Ye, B. Zhu, J. Luo, J. X. Chen, G. Lakshminarayana, and J. R. Qiu, Opt. Exp. **16**, 8989 (2008).
[12] Q. Wang, B. Yang, Y. Zhang, H. Xia, T. Zhao, and H. J iang, J. Alloy Compd. **581**, 801 (2013).
[13] T. Tsuboi, H. Murayama, and K. Shimamura, J. Alloy Compd. **408/412**, 776 (2006).
[14] J. Klafter and M. F. Shlesinger, Proc. Natl. Acad. Sci. USA **83**, 848 (1986).
[15] M. Inokuti and F. Hirayama, J. Chem. Phys. **43**, 1978 (1965).

DOI:10.1063/1674-0068/28/cjcp1407115